

Development of permanent magnet materials—from the view point of first-principles calculation

Hisazumi AKAI¹ and Shinji TSUNEYUKI²

¹*The Institute for Solid State Physics, The University of Tokyo
Kashiwa-no-ha, Kashiwa, Chiba 277-8581, Japan*

²*Graduate School of Science, The University of Tokyo
Hongo, Bunkyo-ku, Tokyo 113-0033, Japan*

Abstract

Theoretical approaches investigating the intrinsic properties of permanent magnet materials are reviewed. Three topics, namely, possible maximum performance of magnetic materials, high-throughput calculation surveying candidates for the high-performance magnetic materials, and the finite temperature magnetic properties, are discussed. Emphasis is put on the importance of large scale first-principles as well as high-throughput calculations.

1 Introduction

The properties featuring high-performance permanent magnets such as $\text{Nd}_2\text{Fe}_{14}\text{B}$ originate from subtle combination of micro, macro and metallographic structures. This means that intrinsic properties of permanent magnet materials are not directly reflected to the properties of permanent magnets. On the other hand, it is also true that the performance of a permanent magnet as a whole is severely limited by the intrinsic properties of constituent materials. For example, the upper bound of coercivity is the magnetocrystalline anisotropy—reality is that it is usually only 20~30% of the latter. Among those intrinsic properties, important ones are, in addition to the magnetocrystalline anisotropy, the magnetic moment and Curie temperature. The higher the values, the better the performance expected. The importance of first-

principle calculation arises here: although predicting the properties of permanent magnets is very difficult task, it would be still possible to predict better materials for permanent magnets on the basis of first-principles calculation. Also, the approach is powerful to analyze the mechanism inherent to certain specific electronic and magnetic properties.

In the past decade, many works based on first-principles calculation have been done from the above point of view [1]. There are two aspects existing in those works: the first one is the accumulation of results of first-principles calculations and their analyses. The second is the development of methodology that enables us to perform such attempts. In this paper, we will present some of our results as examples of the former, putting emphasis upon the importance of the latter.

We first will discuss the possible maximum performance of permanent magnet on the basis of the first principles calculation [2]. In spite of the intensive efforts, no essentially novel magnet showing better performance than $\text{Nd}_2\text{Fe}_{14}\text{B}$ magnet has been so far invented. Then, one might question if there exists any permanent magnet materials at all superior to the already known ones. Or, might it be better to proceed to other directions such as pursuing magnets less expensive but with reasonable performance, and hence, replacing ferrite magnets? In answering this, we will show that there exists a possible maximum performance that we can expect for permanent magnets. Fortunately, this maximum has not been reached by currently used permanent

magnet materials and it is worthwhile seeking further possibilities.

One of ways to seek such possibilities may be performing first-principles calculation over a wide range of composition space of magnetic materials. Since most of those materials contain more than several elements, in many cases as solid solutions, the procedure inevitably becomes a high-dimensional search requiring high-throughput calculations. A machinery based on the Korringa–Kohn–Rostoker Green’s function method combined with the coherent potential approximation (KKR-CPA) is quite efficient for this purpose [3].

For the high throughput calculations, it is desirable to perform calculations for many systems with different compositions in parallel. We have devised such a system, called HOFMAN, which realizes this procedure for KKR-CPA efficiently and have been applied to various systems. Some examples will be given in a later section.

The problem arising in first-principles calculations of rare-earth permanent magnets is a treatment of f -states playing a main role in provoking the magnetocrystalline anisotropy. In the local density approximation (LDA), or the generalized gradient approximation (GGA), the strongly localized f -states cannot be treated properly. So far, no real solution for this problem exists. As a compromise, one may use the exact-exchange [4] instead of the LDA/GGA exchange. Since the f -states in rare-earth elements are sufficiently localized, the exchange energy for f -states may be replaced with that of local f -orbitals. This can be simply done by subtracting self-interaction from the Hartree energy—self-interaction correction (SIC) [5]—because the exchange in the present case is mostly the self-exchange.

The permanent magnets in electric vehicles and wind turbines are used mostly at temperatures 100~200° higher than the room temperature. Therefore, the importance is on the performance at rather high temperatures. Although finite temperature magnetic properties of materials is out of the scope of Kohn–Sham scheme, we can still access this problem through perturbative ways. Namely, we

can estimate the effects of low lying excitation by constructing a low energy effective Hamiltonian through DFT as a problem of the ground state of constrained systems [6]. The results of such calculations give rise to a set of parameters for the effective Hamiltonian, from which we can obtain the finite temperature electronic and magnetic properties.

There are several kinds of excitations that have to be taken into account when discussing finite temperature magnetic properties of magnetic materials. Among them are phonons and magnons [7, 8, 9]. Usually, single electron excitations at the Fermi surfaces do not contribute significantly to the magnetic properties at the temperature range below the Curie temperature. In the following we neglect such excitations. The treatment of phonons is the following: We apply a static approximation for phonons and treat them as external field acting on electrons. This problem can be treated in the framework of DFT. The statistical average can be taken, in principle, by performing a functional integral with suitable probability weights. However, this being practically impossible, we further introduce an approximation to make it tractable. We employ a single-site approximation, where the functional integral is reduced to a configuration average using CPA. In this scheme, the effects of phonons are nothing but those of random displacements of atoms around their equilibrium positions. The average displacements are estimated from either the Debye model or first-principles phonon calculations: no noticeable difference between them was found.

The treatment of magnons is somewhat subtle because the motion of the magnetic moments has to be separated from the electron degrees of freedom. We rely on the fact that the time scale of local spin fluctuations is much slower than that of remaining dynamics. Then we can expand the magnetic energy into the local spin fluctuations as

$$E_{\text{mag}}[\mathbf{S}(\mathbf{r})] = -\frac{1}{2} \iint d\mathbf{r} d\mathbf{r}' \mathbf{S}(\mathbf{r}) \chi(\mathbf{r})^{-1} \chi(\mathbf{r}, \mathbf{r}') \chi(\mathbf{r}')^{-1} \mathbf{S}(\mathbf{r}'), \quad (1)$$

where $\mathbf{S}(\mathbf{r})$ is the spin density, $\chi(\mathbf{r})$ and $\chi(\mathbf{r}, \mathbf{r}')$

are the local and non-local susceptibilities, respectively. Such an expansion can be performed in the framework of constrained DFT as long as the above separation of degrees of freedom and the static approximation are employed. This provides us with a low energy effective Hamiltonian of the system, as is already mentioned. If the longitudinal fluctuations neglected, it is nothing but the Heisenberg Hamiltonian. Now, we can take the same approach as used for phonons: instead of random displacement of atoms, random flipping of the local magnetic moments with probability determined self-consistently at each temperature is considered within KKR-CPA.

We have studied the effects of phonons and magnons on finite temperature magnetism, targeting at permanent magnet materials.

We discuss the possible maximum performance of permanent magnets in Sec. 2. Several examples of high-throughput calculation are presented in Sec. 3. Section 4 is devoted for the finite temperature properties of magnetic materials under the existences of phonons and magnons. We summarize in Sec. 5.

2 Maximum performance of permanent magnet materials

We assume that $3d$ magnetic ions are the main origin of magnetic polarization (magnetization). On the other hand, $4f$ ions are of main concern for the magnetic anisotropy energy (MAE) although $3d$ – $5d$ transition metal ions partly contribute to it, in particular, at high temperature. For this reason, we will discuss MAE in a somewhat different way than we do for the magnetic polarization J_S and Curie temperature T_C . The discussions are based on all-electron first-principles electronic structure calculations performed within the framework of the local density approximation (LDA/GGA) of density functional theory (DFT). We used a KKR-CPA package (AkaiKKR) [3], and for the calculation of T_C , Liechtenstein's method [10] was exploited.

Figure 1 shows the overall behavior of magnetic moment $M(a, Z)$ per atom of $3d$ elements plotted

against the lattice constant a and atomic number Z . The crystal structure is fixed to bcc. Here, the fractional atomic number of a fictitious atom is used: $Z = 25, 26$, and 27 corresponds to Mn, Fe, and Co atoms, respectively. Whereas M is a decreasing function of Z for a large lattice constant ($a \sim 3.2 \text{ \AA}$), it shows a usual Slater-Pauling type behavior [11] for a lattice constant of bcc Fe (2.867 \AA at room temperature): it takes the maximum value of $2.35 \mu_B/\text{atom}$ at $Z = 26.2$ and decreases to both sides. The peak position shifts towards larger Z with decreasing lattice constant. Meanwhile, the peak height decreases rapidly. These behaviors are the results of the facts: (1) the position where the transition from strong to weak ferromagnetism takes place is shifted, and (2) the position where the instability of ferromagnetism against volume collapse takes place is shifted, both occurring when atomic number decreases.

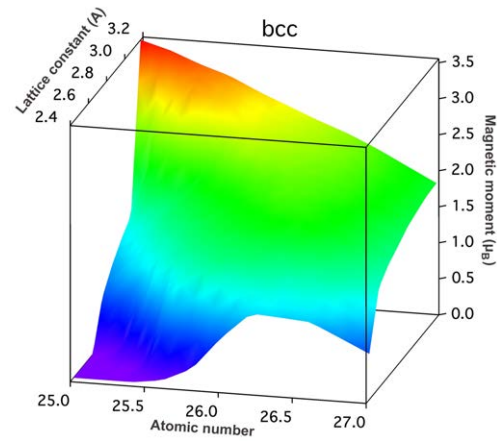


Figure 1: Magnetic moment per atom M against the lattice constant $a(\text{\AA})$ and the atomic number Z of a fictitious atom

The behavior of saturation magnetic polarization J_S shown in Fig. 2 does not obey that of the magnetic moment. The most prominent feature is that it has a dome-like structure appearing around $a = 2.65 \text{ \AA}$ and $z=26.4$, where J_S takes the maximum value of 2.66 T . Such a feature is not seen in M . We point out, not going into details, that this is related to the fact that in the bcc structure, the interatomic distance between nearest neighbor pairs is rather small, forming a considerable bonding–

antibonding splitting and the associated pseudo gap. Unfortunately, the lattice constant $a = 2.65 \text{ \AA}$ is 7 % too small compared with the equilibrium lattice constant of bcc Fe. It should be noticed that, contrary to the behavior of the magnetic moment, the magnetic polarization increases with decreasing a up to the point where the magnetic state starts to rapidly collapse.

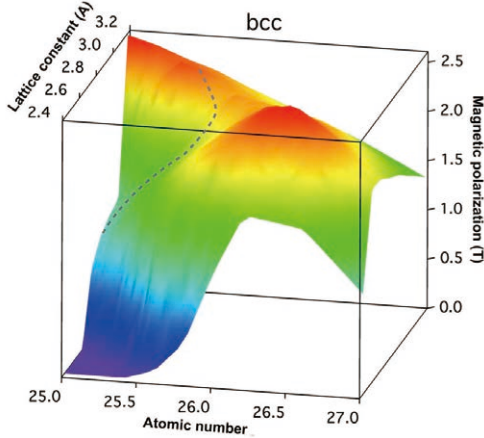


Figure 2: Saturation magnetic polarization J_S of the system against the lattice constant a (\AA) and the atomic number Z of a fictitious atom. The ferromagnetic state is unstable in the region to the left of the dashed line.

Magnetic polarization takes on a large value at one of the corner points in the Z - a plane, $Z = 25$ and $a = 3.2 \text{ \AA}$, but this is not real. The truth is that in a broad region of the Z - a plane—the region to the left of the dashed line in Fig. 2—the ferromagnetic state is unstable as will be seen below. If we combine this fact with the information given by Fig. 2, we may conclude that a large J_S is expected only in the vicinity of the dome-like structure seen in Fig. 2, and the upper limit of J_S would not exceed $\sim 2.7 \text{ T}$.

Figure 3 shows the overall behavior of magnetic transition temperature T_C . Here, we again see a dome-like structure near $Z = 26.5$ and $a = 2.9 \text{ \AA}$. This position approximately coincides with the position of the similar dome-like structure in J_S . This indicates that if $Z = 26.5$ and $a = 2.9 \text{ \AA}$ is forced by some means (crystal structure, chemical composition, pressure, temperature, etc.), $J_S \sim 2.7 \text{ T}$

is achieved. T_C drops rapidly toward the corner in the Z - a plane, $Z = 25$ and $a = 3.2 \text{ \AA}$, where T_C becomes negative, meaning that the antiferromagnetic state should be the ground state. Although the region of stable ferromagnetism does not appear to be extensive, there is hope in the fact that, in most of the region where the ferromagnetism is stable, T_C is well above 1000 K, which is much higher than the usual working temperature range. Now, we may say that the upper limit of T_C is $\sim 2000 \text{ K}$ (if fcc structure were assumed, the upper limit would be $\sim 1500 \text{ K}$).

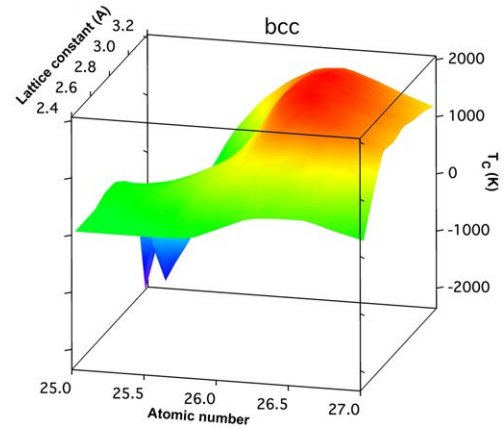


Figure 3: Magnetic transition temperature T_C against the lattice constant a (\AA) and atomic number Z of a fictitious atom. The negative value of T_C means that the antiferromagnetic state is more stable than the ferromagnetic state.

There are two origins of MAE: one is spin orbit coupling and the other is magnetic shape anisotropy. The magnetic shape anisotropy is caused by the dipole interactions between two magnetic moments. In the case of rare earths, the former is the main origin of MAE and is well described within each LS multiplet by the effective Hamiltonian given by $H_{so} = \lambda \mathbf{L} \cdot \mathbf{S}$, where $\lambda = \pm \zeta / n$ is the spin-orbit coupling constant for the ground state LS multiplet. The plus sign is for the less-than-half-filled f shell and vice versa; ζ is the single electron spin-orbit coupling constant, n the number of unpaired electrons. For the $3d$ - $5d$ cases, we use the single electron spin-orbit interactions given by $H_{so} = \sum_i \zeta_i \ell_i \cdot s_i$, where the sum is over

	ζ (eV)			
	s	p	d	f
Fe	8.18	0.231	0.068	0.001
Sm	10.0	1.36	0.218	0.163
Pt	44.2	2.72	0.762	0.001

Table 1: Absolute values of the single electron spin-orbit coupling ζ (eV) of element materials Fe, Sm, and Pt. ζ at the Fermi energy are given.

all electrons. Table 1 shows the values of the spin-orbit coupling constant ζ for some representative elements.

Assuming that the orbitals are firmly bound to the lattice, the upper limit of the magnetic anisotropy constant K_1 for Sm (Sm^{3+} in Sm-type Sm element) estimated from the value of ζ , together with the values of $\langle L \rangle$, is as large as $\sim 1000 \text{ MJm}^{-3}$. The upper limit of K_1 for other lanthanides, if scaled by the value of L , also would be similar to the Sm case. This value obtained under the assumption that the $4f$ orbitals are firmly bound to the lattice, however, seems too large: one order of magnitude smaller, i.e., $\sim 100 \text{ MJm}^{-3}$ would be realistic.

3 High-throughput calculation

The purpose of high-throughput calculation in the present context is to generate data of intrinsic properties of magnetic materials spreading over multi-dimensional composition space. This enable us to construct permanent magnet materials databases that might be used to find new candidates of high-performance permanent magnet materials. Given a structure and a set of components, e.g., $\text{Sm}(\text{Fe}_{1-x}\text{Co}_x)_{12}(\text{N}_{1-y}\text{S}_y)$, we typically need calculations for 100~1000 different systems. Since these systems are compositionally disordered, usual band structure calculation is not sensible. An efficient way to manage this problem is to use the KKR-CPA method [3], which can take a configurational average of disordered systems rather accurately. Unfortunately, the full-potential

scheme is not implemented in the present version of KKR-CPA—full-potential KKR-CPA codes (FP-KKR) exist but they do not suit the high-throughput calculation because of the heavy computational demands. On the other hand, the pseudo-potential codes can calculate the ordered system quite efficiently although their accuracy has to be checked from time to time through comparisons with the results obtained by other reliable method such as FPKKR and FLAPW. Considering the above, one of the practical ways to do is to combine KKR-CPA and pseudo-potential codes: use pseudo-potential codes for the end points, i.e., ordered alloys, of composition space and use KKR-CPA to interpolate whole the region of composition space. A computational system HOFMAN constructed under such a strategy is now running.

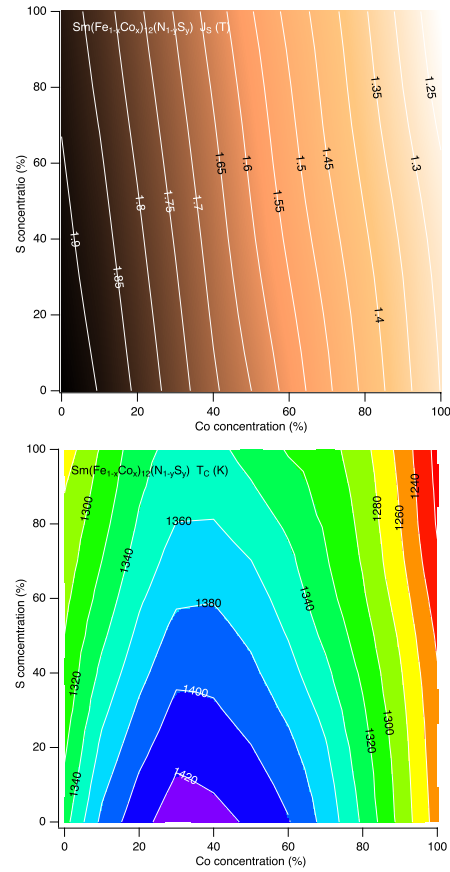


Figure 4: Magnetic polarization (T) (top) and T_C (K) (bottom) of $\text{Sm}(\text{Fe}_{1-x}\text{Co}_x)_{12}(\text{N}_{1-y}\text{S}_y)$.

An example of the usage of HOFMAN system is seen in Fig. 4, where a new alloy system

$\text{Sm}(\text{Fe}_{1-x}\text{Co}_x)_{12}(\text{N}_{1-y}\text{S}_y)$ is examined. The results show that the Curie temperature rises by replacing Fe with Co by $\sim 40\%$ whereas it decreases the magnetic polarization. On the other hand, replacing N with S turned out not to be promising as for the magnetic properties.

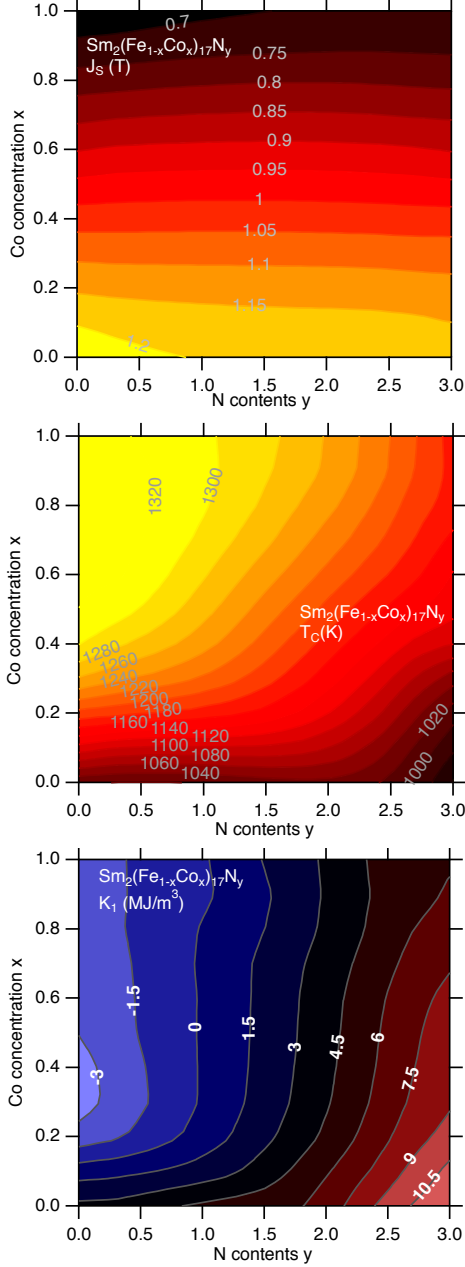


Figure 5: Magnetic polarization (T) (top) and T_C (K) (middle), and K_1 (MJ/m^3) (bottom) of $\text{Sm}(\text{Fe}_{1-x}\text{Co}_x)_{12}\text{N}_y$.

Another example is for $\text{Sm}_2(\text{Fe}_{1-x}\text{Co}_x)_{17}\text{N}_y$,

where the content of N y takes $0 \leq y \leq 3$ (Fig. 5). Here the magnetic anisotropy constant K_1 was also calculated. In this case, T_C monotonically increases as the concentration of Co increases. Although the addition of N lowers T_C , it enhances the uniaxial magnetic anisotropy K_1 . This fact was already known for $\text{Sm}_2\text{Fe}_{17}\text{N}_y$ but addition of Co further enhances this tendency is a new finding.

4 Finite temperature properties of permanent magnet materials

There are many cases that there exist experimental data of magnetic polarization J_S at several different temperatures around the room temperature. What we would like to do is to estimate the temperature dependence of J_S in whole the range of temperature below T_C from these rather restricted data. One of the ways to do this is the following: First, the Curie temperatures, which are not necessarily known experimentally, are estimated by fitting the temperature dependence of magnetic moment by Kuz'min's empirical formula [12]. Meanwhile, the theoretical Curie temperature and 0K magnetic moment are obtained by first-principles calculation using KKR-CPA. Then theoretical temperature dependence of magnetization is obtained again using Kuz'min's formula. Finally, the temperatures are scaled using experimentally estimated Curie temperatures. Examples of such estimation of temperature dependence of J_S are depicted in Fig. 6 for SmFe_{12} family with several different compositions. The theoretical estimations reasonably fit the experimental data and also provide the extrapolation to the whole range of temperature.

Before entering the discussion of the temperature dependence of magnetic properties including the effects of phonons and magnons, it might be useful to see the effects of magnon excitations to the Curie temperature. Such effects comes in through the parameters $\iint d\mathbf{r}d\mathbf{r}' \mathbf{S}(\mathbf{r}) \chi(\mathbf{r})^{-1} \chi(\mathbf{r}, \mathbf{r}') \chi(\mathbf{r}')^{-1} \mathbf{S}(\mathbf{r}') = J_{ij}$ in eq. (1). Here the integral are performed within each atomic cell surrounding i -th or j -th atom. There are two limiting cases in the calculations of

J_{ij} : one is the calculation at the ground state and another is the calculation above T_C where the directions of local moments align randomly without any short-range order. Which is more realistic depends on the characteristic of the spin-fluctuations. The former is realistic for the system where the local fluctuation of the magnetic moments does not play a role. The latter is suitable for the opposite cases.

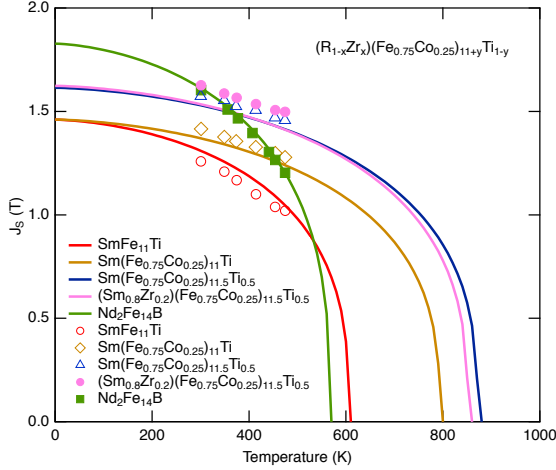
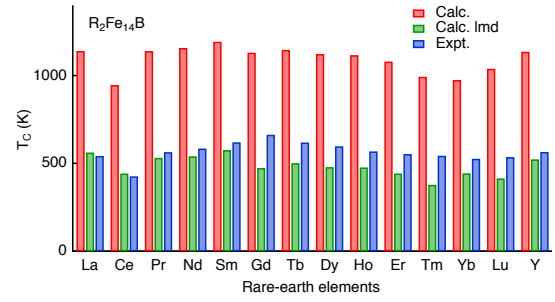


Figure 6: Temperature dependence of magnetization of various systems of SmFe_{12} family.

Figures 7 and 8 show the results of calculation of T_C of $R_2(\text{Fe},\text{Co})_{14}\text{B}$ ($R = \text{La}, \text{Ce}, \dots, \text{Lu}, \text{Y}$). The results under the above two options are compared with the experiments. For the Fe based cases, the calculation assuming that the local fluctuation is dominant (red) gives good agreement with the experiments (blue) whereas the assumption that the long range fluctuation determined T_C (green) seems very reasonable for Co cases.

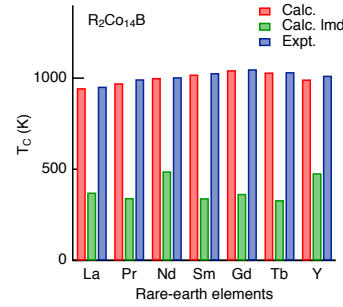
The above discussion is only for T_C with magnons excitations. For the finite temperature properties below T_C and also with not only magnons but also phonons need more elaborate treatment as mentioned in Sec. 1.

	phonons only	plus magnons
0K	1062K	561K
500K	1198K	548K



th]

Figure 7: Calculated T_C of $R_2\text{Fe}_{14}\text{B}$ compared with experiments.



th]

Figure 8: Calculated T_C of $R_2\text{Co}_{14}\text{B}$ compared with experiments.

It was found that, in the case of bcc Fe, there is a significant effect of electron–phonon scattering on the Curie temperature T_C , while that of magnons is not prominent (not shown). On the other hand, the effect of magnons, becomes remarkable in the case of $\text{Nd}_2\text{Fe}_{14}\text{B}$ permanent magnet materials. Some examples of calculated T_C of $\text{Nd}_2\text{Fe}_{14}\text{B}$ are given in Table 2. The first column indicates the temperature in which the average displacement due to phonons is calculated. The experimental value of T_C is 585K.

Figure 9 shows the calculated magnetic polarization of $\text{Nd}_2\text{Fe}_{14}\text{B}$. Both the effects of phonons and magnons are included. The theoretical curve shows a weak first-order transition at the magnetic transition temperature, which occurs as a result of electron–phonon coupling. The temperature is scaled so that T_C reproduces the experimental value of 585K although the scaling factor is close to 1. The calculated results are fairly consistent with experiments, is concluded.

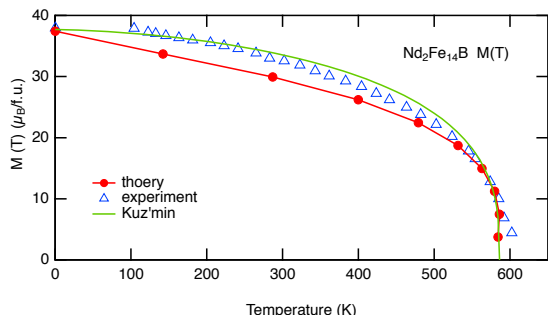


Figure 9: Calculated and experimental magnetic polarization vs. temperature of $\text{Nd}_2\text{Fe}_{14}\text{B}$

5 Summary

We discuss the theoretical approach to investigate the intrinsic properties of permanent magnet materials, focusing on three subjects: possible maximum performance of magnetic materials, high-throughput calculation to survey the candidate of the high-performance magnetic materials in multi-dimensional composition space, and the finite temperature magnetic properties. Admittedly, we have not yet succeeded in inventing any new permanent magnet materials that realize the performance exceeding that of $\text{Nd}_2\text{Fe}_{14}\text{B}$, the best permanent magnet materials so far known. However, we put emphasis on the fact that the remaining composition space not yet searched is immensely large and we still have much chance to get a leap. For this, large scale first-principle calculation such as reviewed here is one of most powerful approaches. In addition, it is clear that schemes fully equipped with machine learning technique provide us with a complementary approach for the development of new permanent magnet materials

References

- [1] See, e.g., T. Miyake, Y. Harashima, T. Fukazawaa, and H. Akai, *Sci. Tech. Adv. Mater.Sci. Tech. Adv. Mater.* **22**, 543 (2021)
- [2] H. Akai, *Scr. Mater.* **154**, 300 (2018).
- [3] H. Akai, AkaiKKR, <http://kkk.issp.u-tokyo.ac.jp/> (2002).
- [4] T. Kotani, *Phys. Rev. B* **50**, 14816 (1994).
- [5] A. Filippetti, C.D. Pemmaraju, S. Sanvito, P. Delugas, D. Puggioni, and V. Fiorentini, *Phys. Rev. B* **84**, 195127 (2011) and references therein.
- [6] P.H. Dederichs, S. Blügel, R. Zeller, and H. Akai, *Phys. Rev. Lett.* **53**, 2512 (1984).
- [7] N. H. Long, M. Ogura, and H. Akai, *Phys. Rev. B* **85**, 224437 (2012).
- [8] S. Kou and H. Akai, *Solid State Commun.* **296**, 1 (2018).
- [9] H. Shinya, S. Kou, T. Fukushima, A. Masago, K. Sato, H. Katayama-Yoshida, and H. Akai, *Appl. Phys. Lett.* **117**, 042402 (2020).
- [10] A. I. Liechtenstein, M. Katsnelson, V. Antropov, V. Gubanov, *J. Magn. Magn. Mater.* **67**, 65 (1987).
- [11] P.H. Dederichs, R. Zeller, H. Akai, and H. Ebert *J. Magn. Magn. Mater.* **100**, 241 (1991).
- [12] M. D. Kuz'min, *Phys. Rev. Lett.* **94**, 107204 (2005).